



ORIGINAL PAPER

INVESTIGATION OF POST INDUCED SEISMIC DEFORMATION OF THE 2016 M_w 4.2 TARNOWEK POLAND MINING TREMOR BASED ON DINSAR AND SBAS METHODS**Wojciech MILCZAREK***Wroclaw University of Science and Technology, Faculty of Geoen지니어ing, Mining and Geology, Wybrzeże Wyspiańskiego 27, 50–370 Wrocław, Poland***Corresponding author's e-mail: wojciech.milczarek@pwr.wroc.pl***ARTICLE INFO****Article history:**

Received 2 January 2019

Accepted 25 March 2019

Available online 24 April 2019

Keywords:

Mining tremors

Subsidence

Satellite radar interferometry

Sentinel 1A/1B

Copper ore mining

ABSTRACT

The article presents an attempt at using synthetic aperture radar interferometry to determine surface displacement in a region affected by a strong earthquake induced by underground mining operations. It was assumed that the satellite radar data obtained from the Sentinel 1A/B satellites may be used to monitor induced seismicity, i.e. mining tremors. Such seismic activity is observed at much shallower depths, and the surface area affected by such activity is much more limited than in the case of natural seismic events. Research was performed in a region located in the southwest part of Poland, where copper ore is extracted using underground methods. The geological structure of the selected area increases the likelihood of induced seismic events. Moreover, the area is one of the most seismically active regions in this part of Europe. The tremor analysed in this paper occurred on November 29, 2016, and had a magnitude of M_w 4.2. Calculations showed that the seismic event resulted in the creation of a 2.7 km x 2.5 km subsidence basin. The paper demonstrates that it is possible to use data provided by the Sentinel 1A/B satellites to detect surface displacements caused by a mining tremor.

INTRODUCTION

From the physical point of view, there is no difference between induced and natural seismicity. Unlike natural earthquakes, however, in most cases, induced tremors have a smaller magnitude and a smaller area affected on the surface. Records of surface vibrations caused by mining tremors show some similarity to vibrations caused by tectonic movements. One of the factors which allow 0.5–2.5 between natural earthquakes and induced tremors is the duration of the strong motion phase (Trifunac and Brady, 1975; Zembaty, 2004). In the case of earthquakes, this time is 20 sec. or more, while in the case of mining tremors, it is 0.5–2.5 sec. Another feature that is characteristic to mining tremors and earthquakes is the size of the affected area. According to (Bohnhoff et al., 2010), tremors that have magnitudes in the ranges of M_w 2–4 and M_w 4–6 may generate surface displacements of 4–40 mm and 4–40 cm, respectively. A particular magnitude range corresponds to the range of induced tremors. In such a case, the changes on the surface may be detectable within a distance of 0.1 to 1 km (M_w 2–4) or 1 to 10 km (M_w 4–6) (Maciąg, 2002). The frequency of surface vibration is another important factor which differentiates natural earthquakes and induced tremors. The dominant surface vibration frequencies from earthquakes are much lower than those from

mining tremors. Maximum acceleration values of vibrations caused by mining tremors are reached within the frequency range of 2.5–12.5 Hz. However, sometimes this frequency range is 18–30 Hz, and occasionally even up to 40 Hz (Maciąg, 2002). In the case of earthquakes, this frequency is no more than several Hz. Induced tremors occur in specific areas, typically limited to regions in which man is intensively working the rock mass (e.g. mining operations, oil and gas extraction or wastewater injection).

Research to date has shown that Synthetic Aperture Radar (SAR) interferometry may be successfully used to measure the influence of earthquakes (on a regional scale) on the land surface (Huang et al., 2017; Lindsey et al., 2015; Tong et al., 2010; Tung and Masterlark, 2016). SAR interferometry is also used to estimate the activity of tectonic faults (Tong et al., 2013; Hussain et al., 2016) and volcanic activity (Henderson and Pritchard, 2013; Remy et al., 2015). It is also employed in research on the influence of underground mining activity on the land surface (Cuenca et al., 2013; Samsonov et al., 2013; Milczarek et al., 2017). Literature offers examples of the use of satellite radar data to evaluate how seismicity induced by such activities as wastewater injection (Yeck et al., 2017), geothermal field monitoring (Vasco et al., 2013; Lin and Wu,

2018), or oil and gas extraction (Verdon et al., 2016) affect the shape of the land surface. Only a limited number of publications, however, describe the use of SAR data in identifying terrain surface changes caused by a mining-induced tremor (Eneva, 2010; Barnhart et al., 2014; Gee et al., 2017; Krawczyk and Grzybek, 2018; Malinowska et al., 2018).

Underground mining causes the equilibrium of the rock mass to be disturbed. In mining regions, fragments of rock mass are displaced into the centers of post-mining voids. Changes also include stress fields. Tremors induced by underground mining operations are referred to as mining tremors. The factors that influence the induced seismic events are: the depth of exploitation, the type of exploitation system, as well as geological and mining conditions. Gibowicz and Kijko (1994) proposed the division of mining tremors into two main types. The first type is characterized by the medium magnitude of the tremor, and the number of tremors is closely related to the intensiveness of the conducted exploitation. The second type of mining tremor is generally more powerful. The range of this type of shock is much larger (on the scale of the mine) and is related to local tectonic discontinuities.

Mining tremors are generated when mining stresses, tectonic stresses and lithostatic stresses overlap. These stresses cause an increase of the potential energy in the rock mass. When the strength limits are exceeded, the rock mass is destroyed and the potential energy is rapidly released. The balance of this process is described by the following equation (Fairhurst and Cornet, 1981):

$$W + Q_0 = U + S + E_k + Q_1 \quad (1)$$

where:

W – work of external forces, Q_0 – thermal energy flowing through the rock mass, S – energy permanently dissipated in the process of rock mass deformation, U – elastic strain energy, E_k – kinetic energy, Q_1 – thermal energy accumulated in the rock. Importantly, a small part of kinetic energy (up to 1 %) is transformed into seismic energy. This energy propagates in the form of elastic waves. Changes of the land surface caused by vibrations due to a tremor may take either a continuous (a subsiding trough) or non-continuous (scarps, sink holes) form. Such phenomena require a number of criteria to be met, which include: (1) a certain depth of mining operations, (2) the presence of thick and strong rock layers which may be transformed, as a result of mining operations, in the so-called layers of potential induced seismic activity, (3) certain tectonics of the deposit, (4) local stress distribution due to mining activity. In the case of tremors induced by underground mining activity, the focus depth rarely exceeds the depth of the mining activity.

Tremors accompany mining operations in many mining basins all around the world, e.g. in Great

Britain (Kusznir et al., 1980), in Germany (Bischoff et al., 2010), in the Republic of South Africa (Riemer and Durrheim, 2012), in the United States (Kubacki et al., 2014), in China (Wang et al., 2015), or in Poland (Drzewiecki and Piernikarczyk, 2017). It should also be mentioned that induced seismicity may be related to gas and oil extraction (Lei et al., 2013; Dempsey and Suckale, 2017), wastewater injection (Talebi, 1998; Fan et al., 2016; McClure et al., 2017), geothermal energy (Diehl et al., 2017; Juncu et al., 2017), extraction of natural gas using hydraulic fracturing (King et al., 2014; Schultz et al., 2015), or water reservoirs (Talebi, 1998). Some works (Grünthal, 2014; Petersen et al., 2015; Grigoli et al., 2017) discuss induced seismicity on a regional/global scale.

In Poland, the problem of mining tremors is related to underground mining carried out in the Upper Silesian Coal Basin (Stec, 2007) and in the Legnica–Glogow Copper Belt (L–GCB) (Orlecka–Sikora et al., 2014), as well as in the open cast lignite mine in the Belchatow Lignite Basin (Gibowicz et al., 1981). The L–GCB region shows the highest level of seismic activity. Lime–dolomite rocks and anhydrites located above the deposit store elastic strain energy and release it as they fracture. As the excavations are located at a great depth (600–1300 m) and performed with the retreat mining method, additional favourable conditions for energy accumulation are created. The strongest seismic events in this area are similar in character to weak earthquakes.

On November 29, 2016, a 4.2 mining tremor was recorded in the area of the “Rudna” mining operation (the L–GCB region). The epicentre of this mining tremor was located near the Zelazny Most reservoir (less than a kilometre from the western slope), between the villages of Komorniki and Tarnówek (Fig. 1). This tremor was one of the strongest recorded in the region in recent years. Directly in the mining tremor region, copper ore exploration 1130 m below the surface was carried out using the room and pillars method.

Since the launch (on April 03, 2014) of the first of the two Sentinel 1 satellites with SAR equipment on board, it has been possible to monitor terrain surface activity on an unprecedented scale. The features of the new radar system allow more detailed results than the results from previous SAR-equipped satellites, especially for areas in which some decorrelation factors have often previously prevented reliable analysis of terrain surface activity. A constellation of two satellites enables surface changes to be detected with a theoretical time interval of 6 days.

To sum up, a sufficiently strong induced seismic event may lead to permanent displacements on the terrain surface. However, as induced seismic events have a geographically limited range, their results are also local. Surface deformations may extend from several hundred meters to several kilometres. With such assumptions taken, the following question arises:

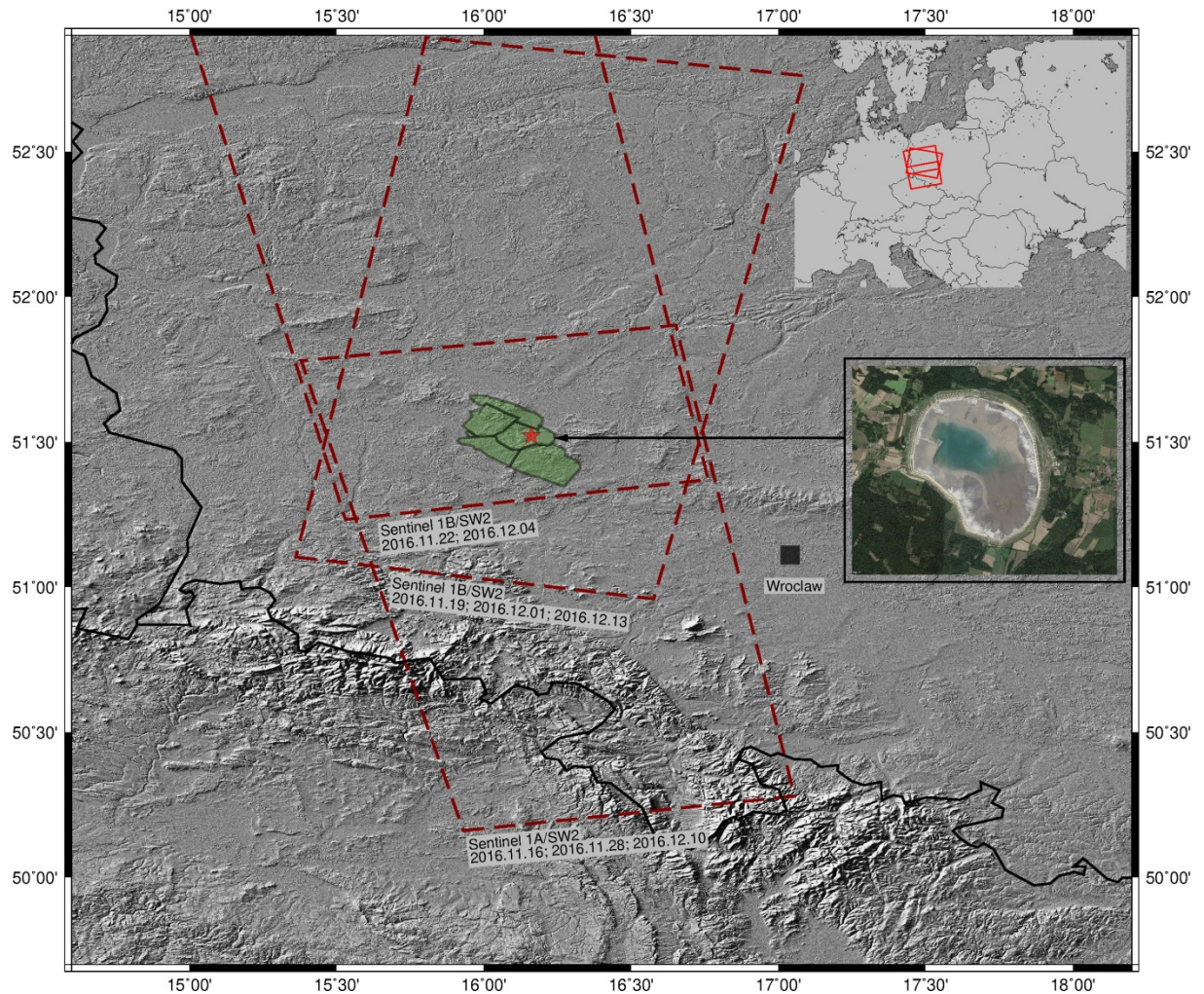


Fig. 1 Location of the induced tremor of Nov. 28, 2016 (red star) The green areas represent the borders of the L–GCB mining region. The areas denoted with the red dashed line correspond to the range of the radar images used in this research (in each case the sub–swath is no. IW2). The upper right corner contains the spatial range of SAR data compared to Central and Eastern Europe. The photograph below shows the Żelazny Most post–floatation tailings reservoir (source: google maps, as of 2018).

is it possible to detect such surface displacements (especially those that are smaller, on the order of several hundred meters) using satellite radar images?

AREA OF STUDY

At present, copper ore is extracted in the L-GCB region in the southwest of Poland (Fig. 1) and at a depth of more than 1100 m below the terrain surface. The L–GCB areas are part of the Fore Sudetic monocline, whose structure was shaped during the Cimmerian and Laramie movements. The base of the monocline consists of metamorphic proterozoic formations (mainly gneisses and amphibolites) which remain at a depth of over 1400 m. The base is also formed of Permian–Mesozoic rocks. The copper ore deposit in this area is located in the roof part of the Rotliegend and in the floor part of the Zechstein. The deposit is one of the biggest polymetallic deposits in the world and has an area of more than 750 km².

The underground mining activity undertaken in the area since the 1960s has significantly disturbed the equilibrium in the rock mass. In effect, a series of disadvantageous phenomena may be observed in the vicinity of the mining area. These phenomena include continuous and non–continuous surface deformations. Apart from surface deformations caused by mineral extraction, mining tremors are also recorded. In the L–GCB region, a total number of 1504 induced seismic events were recorded between 2000 and the end of 2016. The vast majority of the tremors (1242) were in the range M_w 2.5 to 3.5. Magnitudes of 3.6 to 4 were calculated for 168 tremors. The strongest tremors, measured between M_w 4.1 to 5.0, accounted for about 6 % (94) of the total number.

Some of the tremors were located dangerously close to the Żelazny Most reservoir – the biggest reservoir in Europe. The construction of this post–floatation tailings reservoir started in 1974. At present,

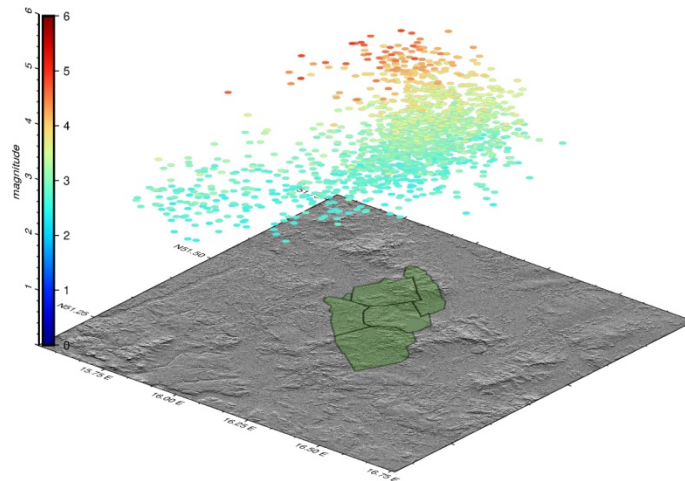


Fig. 2 Spatial distribution of mining tremors with a magnitude greater than 2.5, recorded in the L–GCB region (the green polygons). The tremor magnitudes of individual seismic events are shown on the vertical scale.

Table 1 Interferograms used in the analysis of the Nov. 28, 2016* - mining tremor, together with basic information.

track no.	Satellite	Reference Date Product/ Time of acquisition (UTC)**	Repeat Date Product/ Time of acquisition (UTC)**	Flight direction	B. perp [m]	Mean Coherence [-]
22	Sentinel 1B	19 Nov 2016/05:08:34	01 Dec 2016/05:08:34	Descending	127	0.37
22	Sentinel 1B	01 Dec 2016/05:08:34	13 Dec 2016/05:08:34	Descending	14	0.29
73	Sentinel 1A	16 Nov 2016/16:38:23	28 Nov 2016/16:38:23	Ascending	42	0.35
73	Sentinel 1A	28 Nov 2016/16:38:23	10 Dec 2016/16:38:23	Ascending	-51	0.44
73	Sentinel 1B	22 Nov 2016/16:38:25	04 Dec 2016/16:38:25	Ascending	-6	0.41

* The analyzed tremor took place at 20:09:39 UTC.

** Time of acquisition in this case means the end of data acquisition for the IW2 sub-swath; in the case of all SAR images used, mean measurement time for the whole IW2 was 31 s.

the total length of the weirs is 14.3 km and the reservoir's total capacity is 440 million m³. Its total surface is 1394 ha and the maximum weir height is 60 m. The Zelazny Most reservoir stores post-flotation tailings from the copper ore concentration process. Although the analyzed tremor was located about 8.5 km from the north weir of the reservoir, the question arises of whether it could have affected the reservoir's structure.

DATA PROCESSING

The analysis of the effects of the mining tremor was based on the radar data obtained from the Sentinel 1A and 1B satellites (Table 1). The main calculations were carried out using the DinSAR differential method (Differential SAR Interferometry). In total, 5 interferograms were calculated that temporarily included the tremor and the periods before and after its occurrence. Such a combination made it possible to

detect possible displacements before and after the tremor.

Due to the fact that copper ore is exploited in the area of the tremor, it was decided to carry out additional calculations using the SBAS time series method. The calculation period covered the entire year 2016. A total of 27 SAR images (Sentinel 1A and 1B) from track no. 73 were used for the calculations. The average period between each acquisition was 12 days. The total number of interferograms was 78 (Fig. 6 – upper). It was assumed that calculations using the SBAS method would allow the exploitation impacts on the surface to be correlated with the shifts that exposed the analyzed tremor.

The data was processed with an updated version of GMTSAR ver. 5.0.0 (Sandwell et al., 2011) with additional post-processing using GMT ver. 5.4.0 (Wessel and Smith, 2013) and Snaphu ver. 1.4.2 to unwrap the interferograms based on the minimum

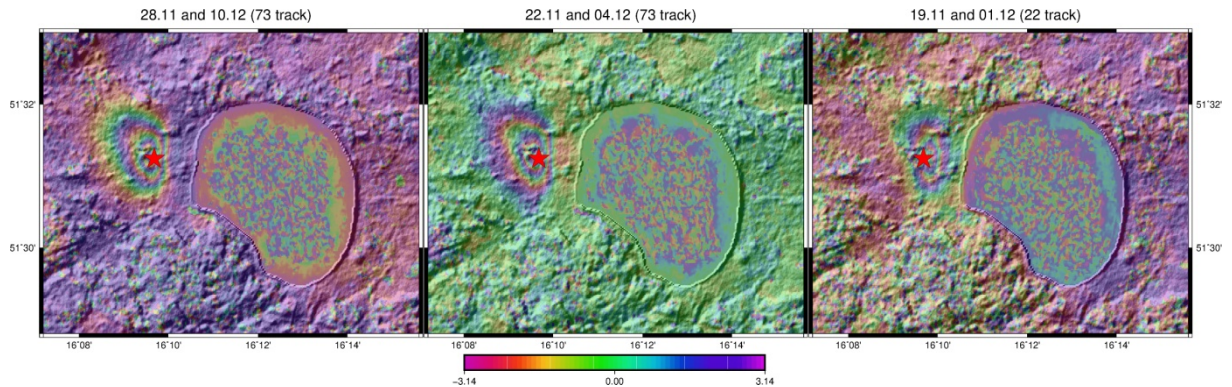


Fig. 3 Examples of a coseismic interferogram from Sentinel 1A/1B related to the induced tremor of Nov. 28, 2016. The subsequent interferograms were calculated on the basis of the following pairs of SAR images (starting on the right side): Nov. 28 to Dec. 10 (track no. 73), Nov. 22 to Dec. 04 (track no. 73) and Nov. 19 to Dec. 01 (track no. 22). The data was processed using GMTSAR (Sandwell et al., 2011). The epicenter of the mining tremor is marked with a red star.

cost flow algorithm (Chen and Zebker, 2000). The calculations on the tremor of Nov. 29, 2016, were based on six radar images from the Sentinel 1A/B satellites operated under the Copernicus program by the European Space Agency (ESA) (the photographs were retrieved from <https://scihub.copernicus.eu/dhus/>). A precise orbit was retrieved for each image (<https://qc.sentinel1.eo.esa.int/>). Wave phase correction in relation to the ground surface was performed with the Shuttle Radar Topography Mission (SRTM) version 1 (Farr et al., 2007) (retrieved from <http://topex.ucsd.edu/gmtsar/demgen/>). The results, in the form of LOS (line-of-sight) values, were geocoded into the World Geodetic System 84 coordinate system. All Figures were prepared using GMT software (ver. 5.4.0). The seismic data covering the seismic events in the mining region for the period 2000–2016 was retrieved from the USGS, Earthquake Hazards Program database (<https://earthquake.usgs.gov/>). The vector versions of the borders of mining areas in the L–GCB region were retrieved from the Central Geological Database, operated by Polish Geological Institute (<http://baza.pgi.gov.pl/>).

RESULTS

In order to precisely analyze the impact of the tremor on the terrain surface, a series of interferograms was calculated on the basis of all available SAR images taken at the time of the seismic event. The lower part of Figure 3 shows the time range of the SAR images used.

The three calculated interferograms are from the time range of the tremor of November 28, 2016 (20:09:39 UTC). These are the following (Fig. 3): Nov. 22 to Dec. 04 (track no. 22, descending; Nov. 28 to Dec. 10 and Nov. 19 to Dec. 01 (track no. 73, ascending). The first two interferograms from path 73

are spatially similar (Fig. 4). The observed tremor has an impact on the terrain surface in the range of 2.65 km in the N–S direction and 1.95 km in the E–W direction. However, the interferogram from path 22 shows a different situation: in this case, the observed range in the N–S direction is about 2.55 km and is similar to the values above. But in the E–W direction, the range difference of about 400 m (1.55 km) is already significant. The differences in the parallel direction should be traced to different data acquisition directions for each of the paths and to a different incidence angle.

The main displacements in the radar line-of-sight (LOS) direction, up to -80 mm, were observed from about 400 m (track no. 22) to about 630 m (track no. 73) from the West side of the base of the Żelazny Most reservoir. The calculations performed for the pair from Nov. 16 to Nov. 28 (track no. 73) did not show any changes (Figs. 1 and 2) on the surface before the tremor occurred. For the two interferometers from path 73 (Nov. 22 to Dec. 04 and Nov. 28 to Dec. 10), which cover the time of the tremor, the observed surface displacements are practically the same. Therefore, it can be assumed that the trough is the result of the analyzed tremor. This assumption is confirmed in the calculated interferograms before the tremor (Nov. 16 to Nov. 28, track no. 73) and after the tremor (Dec. 01 to Dec. 13, track no. 22).

In order to allow a precise analysis of the character of the observed displacements, a series of cross sections were generated along selected directions. The A–A' section is in the E–W direction and has a length of 3000 m; the B–B' section, about 3600 m in length, extends along the longest edge (NW–SE) of the created subsidence trough observed in the interferograms from path 73: Nov. 22 to Dec. 04 and Nov. 28 to Dec. 10. The remaining two sections: C–C and D–D (about 4500 m) extend in the

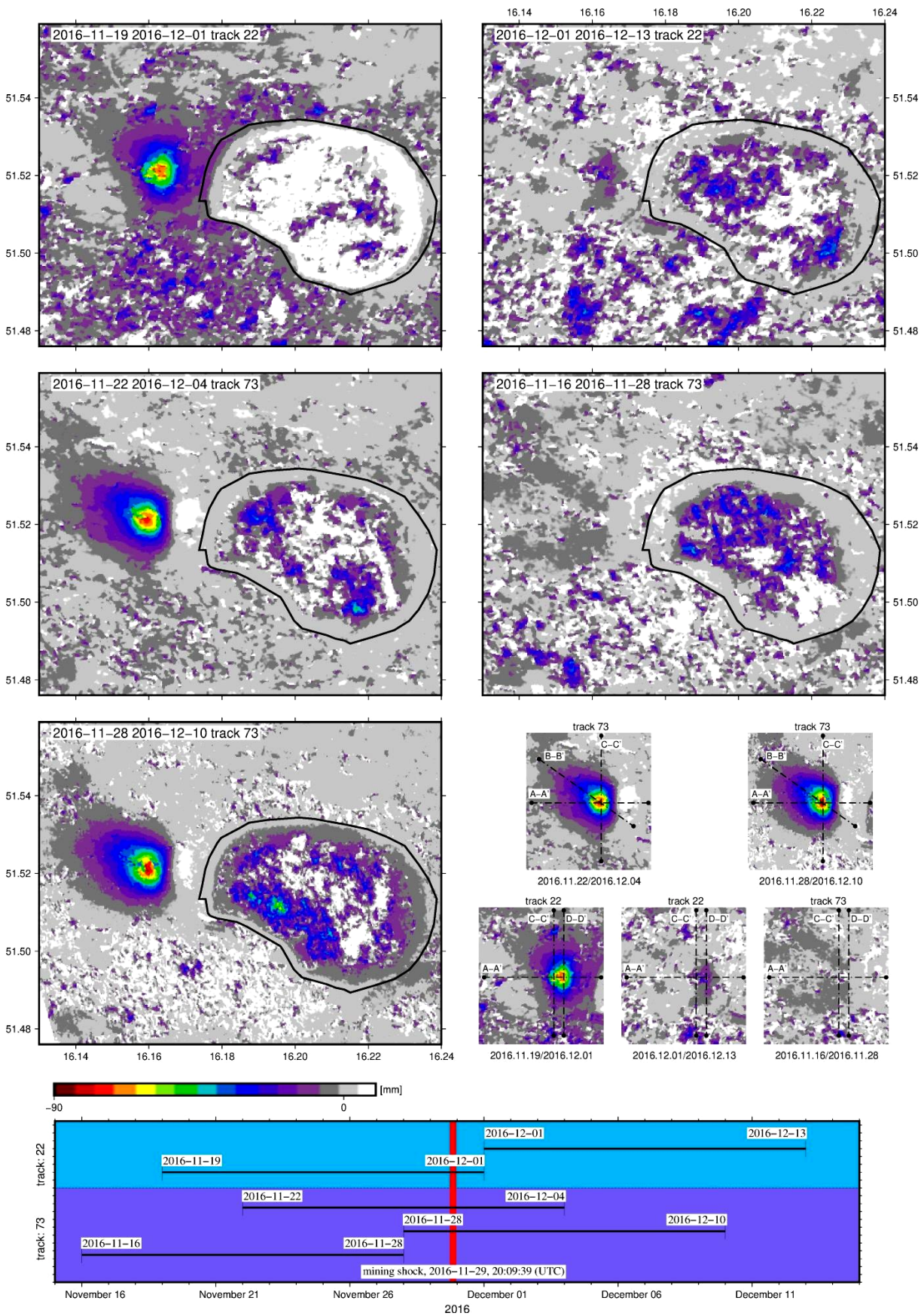


Fig. 4 The LOS displacements (in mm) calculated from subsequent interferograms. The five main maps include, in their top left corners, the dates of the SAR images used for displacement calculations. The black contour denotes the Želazny Most post-flotation tailings reservoir. On the right, the location of subsequent profiles is provided: A-A', B-B', C-C', D-D'. The bottom part of the image shows the distribution of subsequent interferograms in time, with regard to the date of the mining tremor (the red vertical line).

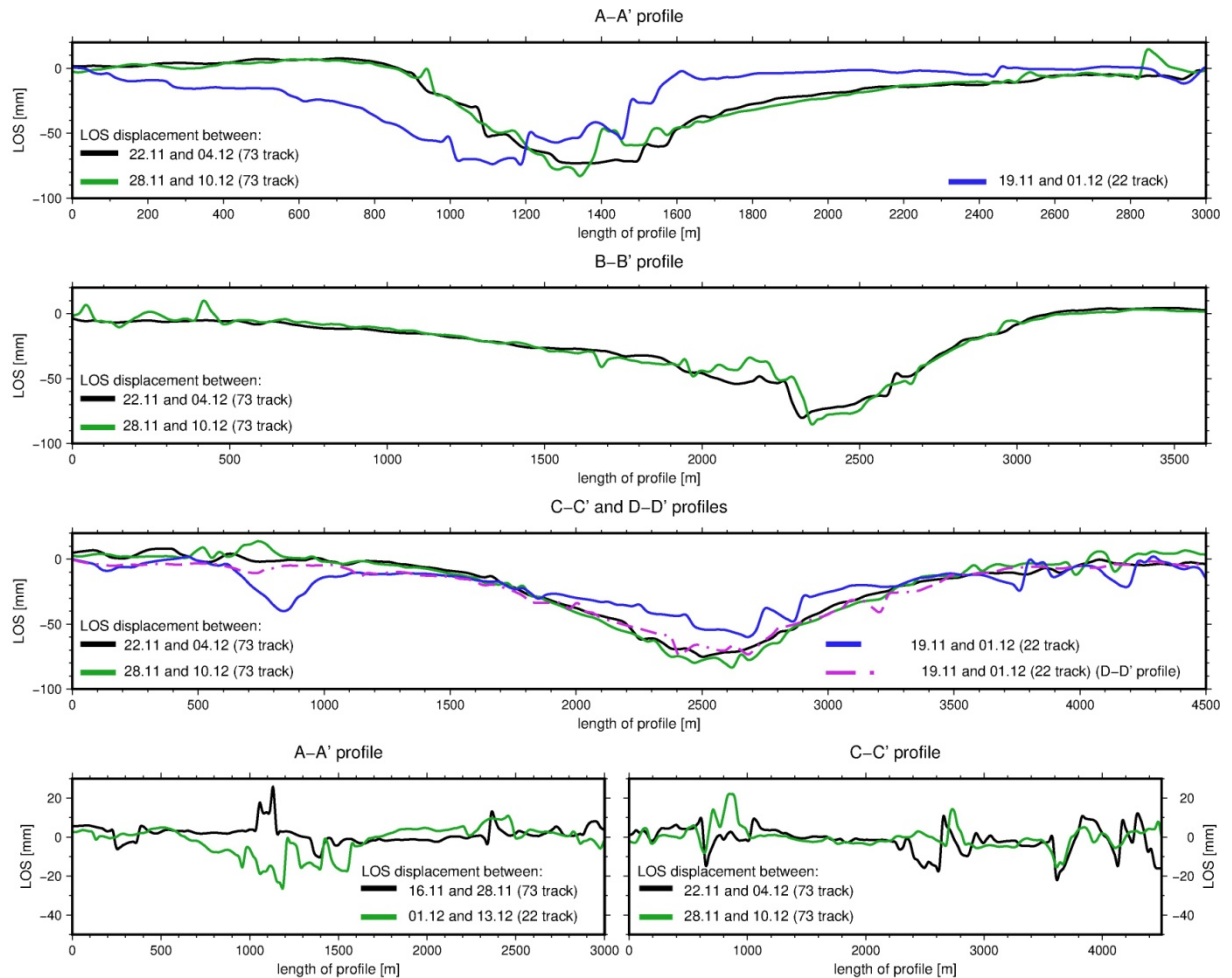


Fig. 5 Profiles of the slopes in the region of the trough created by the induced tremor. The A–A' profile is oriented in the E–W direction, the B–B' profile is in the NW–SE direction, and the C–C' and the D–D' profiles are in the N–S direction. The shift of the D–D' profile in relation to the C–C' profile is 445 m.

N–S direction. The C–C' section cuts centrally across the trough which is visible in the interferograms from path 73. The last section (D–D') cuts centrally across the trough from the Nov. 19 to Dec. 01 interferogram (track no. 22). The shift between the C–C' and D–D' profiles is 445 m.

In the case of the two interferograms from path 73, which cover the time of the analyzed tremor, the maximum terrain subsidence of -80 mm is practically the same. The trough profiles in the analyzed directions (N–S, E–W and NW–SE) show a high consistency. They may allow the conclusion that both before the tremor (7 days) and after it (15 days), no additional changes occurred on the terrain surface in this direction. The results for the remaining analyzed directions (N–S and NW–SE) are similar (Fig. 5).

Comparison of the results from paths 22 and 72 clearly shows the influence of the satellite's direction of flight and hence also the influence of the indicated angle values. The maximum values are preserved, but when the trough from path 22 (Nov. 19 – Dec. 01) is shifted in a parallel direction (the A–A' profile) to path 73, it is about 200 m. A similar observation is

possible when comparing the profiles from paths 73 (C–C') and 22 (D–D') along the N–S direction. The C–C' profile extends across the maximum of the trough that is determined on the basis of the interferograms from path 73, while the D–D' profile is shifted with respect to the previous profile by 450 m to the East and cuts across the trough calculated on the basis of the interferogram from path 22. With such an assumption, the N–S profiles determined from the three interferograms describe a practically identical slope of the trough (Fig. 5).

Based on the two remaining interferograms (Nov. 16 to Nov. 28 and Dec. 01 to Dec. 13), the LOS displacement was calculated for two periods: before the tremor and after the tremor. When analyzing the diagrams (Fig. 5) of the profiles along the two main directions, it is possible to demonstrate that apart from some local noise – there are no significant displacements for the investigated period.

The results obtained by the SBAS method indicate that in the mining tremor region a subsidence basin has been formed during the whole 2016. In the period between November 28 and December 10, there

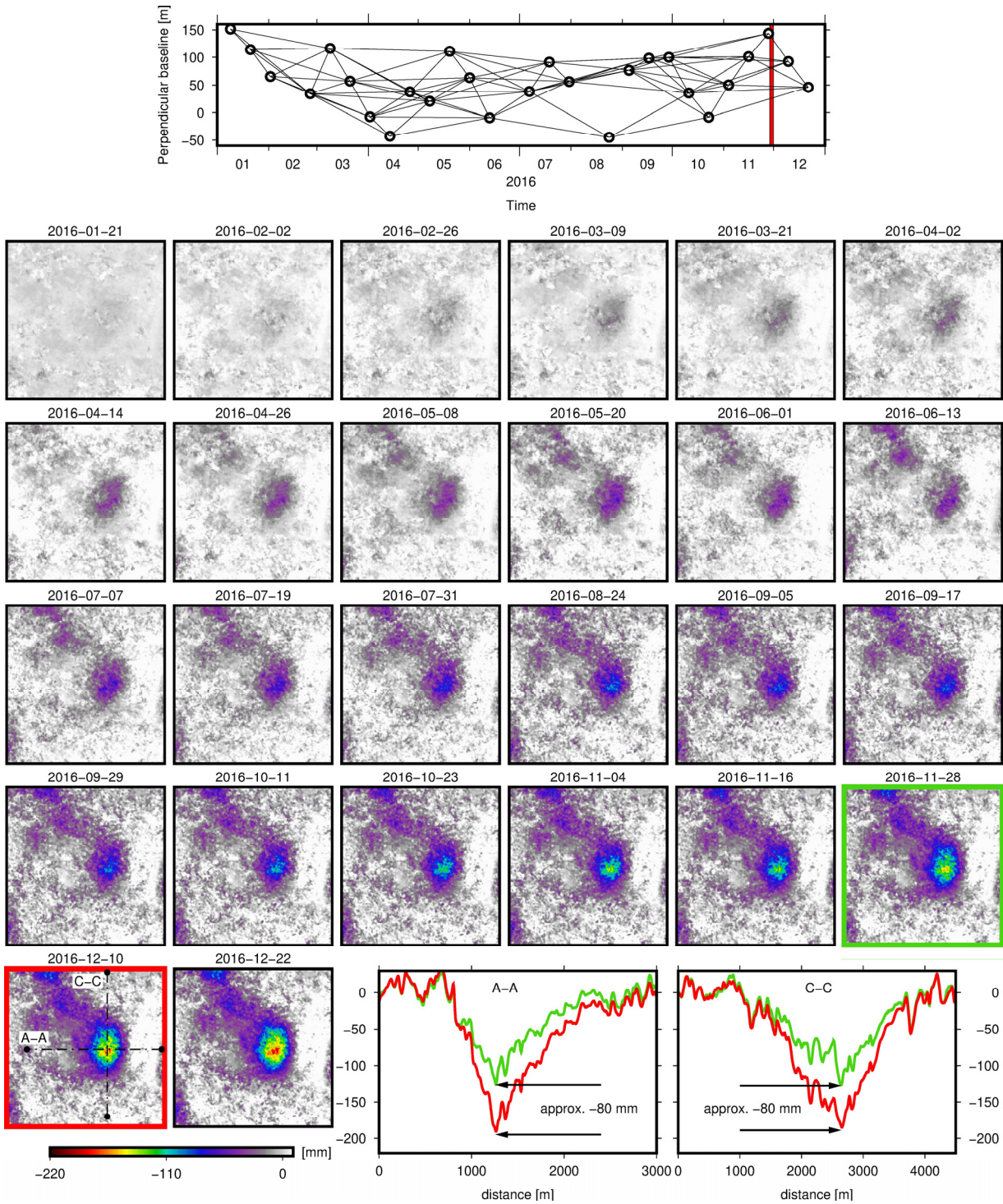


Fig. 6 LOS dislocations were determined in the area of the analyzed mining tremor based on the SBAS method. At the top, a combination of 78 interferograms calculated for all of 2016 is presented. The date of the tremor is marked with a red line. The next LOS displacements (in mm) in 2016 are presented for 26 periods. Maps with green and red envelopes indicate the periods immediately before and after the tremor of November 2016. The diagrams show the displacements for the same cross-sections (A-A and C-C) as were used for the DInSAR calculation (Fig. 5).

was a sharp subsidence in the tremor area of the whole year. The maximum subsidence observed on the A–A and C–C profiles was approximately –80 mm (Fig. 6). SBAS results are consistent with previously presented results obtained by the DInSAR method. The spatial range of subsidence of the tremor coincides with the existing mining subsidence basin.

DISCUSSION AND CONCLUSIONS

The results of this research are consistent with the results offered by Barnhart et al. (2014). They demonstrate that it is possible to use radar data from the Sentinel 1A/B satellites to detect displacements of terrain surface which occur as a result of strong mining tremor (induced events). Based on the presented results, the following final conclusions were formulated.

However, the displacements detected in this research cover a greater geographical range than the results of previous research (Barnhart et al., 2014). The borders of the subsidence trough that was created as a result of the tremor – are clearly visible in the ascending and descending Sentinel–1 interferograms (Fig. 3). In the case of the interferograms from path 73, the dimensions of the trough were 2.65 (in the N–S direction) x 1.95 km (in the E–W direction), and in the case of the interferogram from path 22, they were respectively 2.55 (in the N–S direction) and 1.55 km (in the E–W direction). The ability to detect surface displacements with such small dimensions demonstrates the potential of SAR data from the Sentinel 1 satellite constellation.

Due to the inability to obtain geodetic data from the tremor region as of today, it is not possible to compare the obtained results precisely. Nevertheless, the presented results coincide with the results obtained by Malinowska et al. (2018), and concerning the same event. In turn, Popiołek et al. (2010) analyzed the mining tremor from 2010, which was much stronger (M_w 4.5). Based on the leveling measurements, the maximum subsidence was estimated at about –150 mm.

Although an attempt was made to observe surface displacements accompanying the Dec. 26, 2016 tremor, no significant additional surface displacements were identified either before or after the analyzed tremor occurred. Taking into account the accuracy of the LOS displacements, it could be concluded that there were no residual movements.

The SBAS calculations clearly showed that the observed displacements coincide with the subsidence basin which is connected with the underground exploitation of copper ore conducted in this area. On this basis, it can be concluded that the induced mining tremor can promote affect the deformation of the ground surface in the area of exploitation.

The location of the tremor occurred exactly in the operating field XXI2 (unit branch G–23) which additionally confirms the induced character of the shock.

Future research will focus on analyzing all mining tremors which occurred in the L–GCB region in order to detect any resulting surface displacements. Analysis of a larger number of cases will allow a better understanding of the influence that induced tremors have on the land surface.

REFERENCES

- Barnhart, W.D., Benz, H.M., Hayes, G.P., Rubinstein, J.L., Bergman, E., Benz, H.M., Hayes, G.P., Rubinstein, J.L. and Bergman, E.: 2014, Seismological and geodetic constraints on the 2011 M_w 5.3 Trinidad, Colorado earthquake and induced deformation in the Raton Basin. *J. Geophys. Res., Solid Earth*, 119, 10, 7923–7933. DOI: 10.1002/2014JB011227
- Bischoff, M., Cete, A., Fritschen, R. and Meier, T.: 2010, Coal mining induced seismicity in the Ruhr area, Germany. *Pure Appl. Geophys.*, 167, 1–2, 63–75. DOI: 10.1007/s00024-009-0001-8
- Bohnhoff, M., Dresen, G., Ellsworth, W.L. and Ito, H.: 2010, Passive seismic monitoring of natural and induced earthquakes: case studies, future directions and socio-economic relevance. IN: Cloetingh, S., Negendank, J. (Eds.), *New Frontiers in Integrated Solid Earth Sciences*. Springer, Dordrecht, New York, 261–285. DOI: 10.1007/978-90-481-2737-5_7
- Caro Cuenca, M., Hooper, A.J. and Hanssen, R.F.: 2013, Surface deformation induced by water influx in the abandoned coal mines in Limburg, The Netherlands observed by satellite radar interferometry. *J. Appl. Geophys.*, 88, 1–11. DOI: 10.1016/j.jappgeo.2012.10.003
- Chen, C.W. and Zebker, H.A.: 2000, Network approaches to two-dimensional phase unwrapping: intractability and two new algorithms. *J. Opt. Soc. Am. A*, 17, 3, 401–414. DOI: 10.1364/JOSAA.17.000401
- Dempsey, D. and Suckale, J.: 2017, Physics-based forecasting of induced seismicity at Groningen gas field, the Netherlands. *Geophys. Res. Lett.*, 44, 15, 7773–7782. DOI: 10.1002/2017GL073878
- Diehl, T., Kraft, T., Kissling, E. and Wiemer, S.: 2017, The induced earthquake sequence related to the St. Gallen deep geothermal project (Switzerland): Fault reactivation and fluid interactions imaged by microseismicity. *J. Geophys. Res., Solid Earth*, 122, 9, 7272–7290. DOI: 10.1002/2017JB014473
- Drzewiecki, J. and Piernikarczyk, A.: 2017, The forecast of mining-induced seismicity and the consequent risk of damage to the excavation in the area of seismic event. *J. Sustain. Min.*, 16, 1–7. DOI: 10.1016/j.jsm.2017.05.001
- Eneva, M.: 2010, Detection of surface deformation at mining and geothermal sites using Satellite Radar Interferometry (InSAR). 44th U.S. Rock Mechanics Symposium and 5th U.S.–Canada Rock Mechanics Symposium, 27–30 June, Salt Lake City, Utah.
- Fairhurst, C. and Cornet, F.: 1981, Rock fracture and fragmentation. IN: *Proc. 22nd U.S. Symp. on Rock Mechanics*, 21–46.
- Fan, Z., Eichhubl, P. and Gale, J.F.W.: 2016, Geomechanical analysis of fluid injection and seismic fault slip for the M_w 4.8 Timpson, Texas, earthquake sequence. *J. Geophys. Res., Solid Earth*, 121, 4, 2798–2812. DOI: 10.1002/2016JB012821

- Farr, T., Rosen, P., Caro, E., Crippen, R., Duren, R., Hensley, S., Kobrick, M., Paller, M., Rodriguez, E., Roth, L., Seal, D., Shaffer, S., Shimada, J., Umland, J., Werner, M., Oskin, M., Burbank, D. and Alsdorf, D.: 2007, The shuttle radar topography mission. *Rev. Geophys.*, 45, 2, 1–33. DOI: 10.1029/2005RG000183
- Gee, D., Bateson, L., Sowter, A. Grebby, S., Novellino, A., Cigna, F., Marsh, S., Banton, C. and Wyatt, L.: 2017, Ground motion in areas of abandoned mining: Application of the Intermittent SBAS (ISBAS) to the Northumberland and Durham Coalfield, UK. *Geosciences*, 7, 3, 85. DOI: 10.3390/geosciences7030085
- Gibowicz, S.J. and Kijko, A.: 1994, An introduction to mining seismology. Academic Press, chapter 2, 15–23.
- Gibowicz, S.J., Droste, Z., Guterch, B. and Hordejuk, J.: 1981, The Belchatow, Poland, earthquakes of 1979 and 1980 induced by surface mining. *Eng. Geol.*, 17, 4, 257–271. DOI: 10.1016/0013-7952(81)90002-8
- Grigoli, F., Cesca, S., Priolo, E., Rinaldi, A.P., Clinton, J.F., Stabile, T.A., Dost, B., Fernandez, M.G., Wiemer, S. and Dahm, T.: 2017, Current challenges in monitoring, discrimination, and management of induced seismicity related to underground industrial activities: A European perspective. *Rev. Geophys.*, 55, 2, 310–340. DOI: 10.1002/2016RG000542
- Grünthal, G.: 2014, Induced seismicity related to geothermal projects versus natural tectonic earthquakes and other types of induced seismic events in Central Europe. *Geothermics*, 52, 22–35. DOI: 10.1016/j.geothermics.2013.09.009
- Henderson, S.T. and Pritchard, M.E.: 2013, Decadal volcanic deformation in the central andes volcanic zone revealed by InSAR time series. *Geochem. Geophys. Geosy.*, 14, 5, 1358–1374. DOI: 10.1002/ggge.20074
- Huang, M.H., Fielding, E.J., Liang, C., Milillo, P., Bekaert, D., Dreger, D. and Salzer, J.: 2017, Coseismic deformation and triggered landslides of the 2016 Mw 6.2 Amatrice earthquake in Italy. *Geophys. Res. Lett.*, 44, 3, 1266–1274. DOI: 10.1002/2016GL071687
- Hussain, E., Hooper, A., Wright, T.J., Walters, R.J. and Bekaert, D.P.S.: 2016, Interseismic strain accumulation across the central North Anatolian Fault from iteratively unwrapped InSAR measurements. *J. Geophys. Res., Solid Earth*, 121, 12, 9000–9019. DOI: 10.1002/2016JB013108
- Jiang, G., Wen, Y., Liu, Y., Xu, X., Fang, L., Chen, G., Gong, M. and Xu, C.: 2015, Joint analysis of the 2014 Kangding, southwest China, earthquake sequence with seismicity relocation and InSAR inversion. *Geophys. Res. Lett.*, 42, 9, 3273–3281. DOI: 10.1002/2015GL063750
- Juncu, D., Árnadóttir, T., Hooper, A. and Gunnarsson, G.: 2017, Anthropogenic and natural ground deformation in the Hengill geothermal area, Iceland. *J. Geophys. Res., Solid Earth*, 122, 1, 692–709. DOI: 10.1002/2016JB013626
- Krawczyk, A. and Grzybek, R.: 2018, An evaluation of processing InSAR Sentinel-1A/B data for correlation of mining subsidence with mining induced tremors in the Upper Silesian Coal Basin (Poland). *E3S Web Conf.*, 26, 00003, DOI: 10.1051/e3sconf/20182600003
- King, V.M., Block, L.V., Yeck, W.L., Wood, C.K. and Derouin, S.: 2014, Geological structure of the Paradox Valley Region, Colorado, and relationship to seismicity induced by deep well injection. *J. Geophys. Res., Solid Earth*, 119, 6, 4955–4978. DOI: 10.1002/2013JB010651
- Kubacki, T., Koper, K.D., Pankow, K.L. and McCarter, M.K.: 2014, Changes in mining-induced seismicity before and after the 2007 Crandall Canyon Mine collapse. *J. Geophys. Res., Solid Earth*, 119, 6, 4876–4889. DOI: 10.1002/2014JB011037
- Kusznir, N.J., Ashwin, D.P. and Bradley, A.G.: 1980, Mining induced seismicity in the North Staffordshire coalfield, England. *Int. J. Rock Mech. Min. Sci. Geomech. Abstr.*, 17, 1, 45–55. DOI: 10.1016/0148-9062(80)90005-4
- Lei, X., Ma, S., Chen, W., Pang, C., Zeng, J., Jiang, B., 2013, A detailed view of the injection-induced seismicity in a natural gas reservoir in Zigong, southwestern Sichuan Basin, China. *J. Geophys. Res., Solid Earth*, 118, 4296–4311. DOI: 10.1002/jgrb.50310
- Lin, G. and Wu, B.: 2018, Seismic velocity structure and characteristics of induced seismicity at the Geysers Geothermal Field, eastern California. *Geothermics*, 71, 225–233. DOI: 10.1016/j.geothermics.2017.10.003
- Lindsey, E.O., Natsuaki, R., Xu, X., Shimada, M., Hashimoto, M., Melgar, D. and Sandwell, D.T.: 2015, Line-of-sight displacement from ALOS-2 interferometry: Mw 7.8 Gorkha Earthquake and Mw 7.3 aftershock. *Geophys. Res. Lett.*, 42, 16, 6655–6661. DOI: 10.1002/2015GL065385
- Maciąg, E.: 2002, Drgania powierzchniowe w LGOM i ich oddziaływanie na zabudowę. IN: XXV Zimowa Szkoła Mechaniki Górniczej, Kraków, 395–410.
- Malinowska, A.A., Witkowski, W.T., Guzy, A. and Hejmanowski, R.: 2018, Mapping ground movements caused by mining-induced earthquakes applying satellite radar interferometry. *Eng. Geol.*, 246, 402–411. DOI: 10.1016/j.enggeo.2018.10.013
- McClure, M., Gibson, R., Chiu, K.K. and Ranganath, R.: 2017, Identifying potentially induced seismicity and assessing statistical significance in Oklahoma and California. *J. Geophys. Res., Solid Earth*, 122, 2153–2172. DOI: 10.1002/2016JB013711
- Milczarek, W., Blachowski, J. and Grzempowski, P.: 2017, Application of PSInSAR for assessment of surface deformations in post-mining area – case study of the former Walbrzych hard coal basin (SW Poland). *Acta Geodyn. Geomater.*, 14, 1(185), 41–52. DOI: 10.13168/AGG.2016.0026
- Orlecka-Sikora, B., Cesca, S., Lasocki, S., Lizurek, G., Wiejacz, P. and Rudzinski, L.: 2014, Seismogenesis of exceptional ground motion due to a sequence of mining induced tremors from Legnica-Głogów Copper District in Poland. *Geophys. J. Int.*, 198, 1, 40–54. DOI: 10.1093/gji/ggu109
- Petersen, B.M.D., Mueller, C.S., Moschetti, M.P., Hoover, S.M., Rubinstein, J.L., Andrea, L., Michael, A.J., Ellsworth, W.L., Mccarr, A.F., Holland, A.A., Anderson, J.G. and Jewell, S.: 2015, Incorporating induced seismicity in the 2014 United States National Seismic Hazard Model — Results of 2014 Workshop and Sensitivity Studies. *USGS Open File Rep.* 2015–1070, 69 pp. DOI: 10.3133/ofr20151070
- Popielek, E., Ostrowski, J., Czaja, J. and Mazur, J.: 2001, The impact of a strong mining tremor on the

- subsidence of the area surface in the Legnica–Glogow Copper Area. 10th FIG Int. Symposium on Deformation Measurements, Orange – California USA, 19–22 March 2001.
- Remy, D., Chen, Y., Froger, J.L., Bonvalot, S., Cordoba, L. and Fustos, J.: 2015, Revised interpretation of recent InSAR signals observed at Llaima volcano (Chile). *Geophys. Res. Lett.*, 42, 10, 3870–3879. DOI: 10.1002/2015GL063872
- Riemer, K.L. and Durrheim, R.J.: 2012, Mining seismicity in the Witwatersrand Basin: monitoring, mechanisms and mitigation strategies in perspective. *J. Rock Mech. Geotech. Eng.*, 4, 3, 228–249. DOI: 10.3724/SP.J.1235.2012.00228
- Samsonov, S., Smets, B., D'Oreye, N. and Smets, B.: 2013, Ground deformation associated with post-mining activity at the French – German border revealed by novel InSAR time series method. *Int. J. Appl. Earth Obs. Geoinf.*, 23, 142–154. DOI: 10.1016/j.jag.2012.12.008
- Sandwell, D., Mellors, R., Tong, X., Wei, M. and Wessel, P.: 2011, Open radar interferometry software for mapping surface deformation. *Eos, Trans. Am. Geophys. Union*, 92, 28, 234. DOI: 10.1029/2011EO280002
- Schultz, R., Stern, V., Novakovic, M., Atkinson, G. and Gu, Y.J.: 2015, Hydraulic fracturing and the Crooked Lake Sequences: Insights gleaned from regional seismic networks. *Geophys. Res. Lett.*, 42, 8, 2750–2758. DOI: 10.1002/2015GL063455
- Stec K.: 2007, Characteristics of seismic activity of the Upper Silesian Coal Basin in Poland. *Geophys. J. Int.*, 168, 2, 757–768. DOI: 10.1111/j.1365–246X.2006.03227.x
- Talebi, S.: 1998, Seismicity associated with mines, reservoirs and fluid injections. *Pure Appl. Geophys.*, 150, 3–4. DOI: 10.1007/978–3–0348–8814–1
- Tong, X., Sandwell, D.T. and Fialko, Y.: 2010, Coseismic slip model of the 2008 Wenchuan earthquake derived from joint inversion of interferometric synthetic aperture radar, GPS, and field data. *J. Geophys. Res.*, 115, B4, B04314. DOI: 10.1029/2009JB006625
- Tong, X., Sandwell, D.T. and Smith–Konter, B.: 2013, High-resolution interseismic velocity data along the San Andreas Fault from GPS and InSAR. *J. Geophys. Res., Solid Earth*, 118, 1, 369–389. DOI: 10.1029/2012JB009442
- Trifunac, M.D. and Brady, A.G.: 1975, A study on the duration of strong earthquake ground motion. *Bull. Seismol. Soc. Am.*, 65, 581–626.
- Tung, S. and Masterlark, T.: 2016, Coseismic slip distribution of the 2015 M_w 7.8 Gorkha, Nepal, earthquake from joint inversion of GPS and InSAR data for slip within a 3–D heterogeneous Domain. *J. Geophys. Res., Solid Earth*, 121, 3479–3503. DOI: 10.1002/2015JB012497
- Vasco, D.W., Rutqvist, J., Ferretti, A., Rucci, A., Bellotti, F., Dobson, P., Oldenburg, C., Garcia, J., Walters, M. and Hartline, C.: 2013, Monitoring deformation at the Geysers geothermal field, California using C–band and X–band interferometric synthetic aperture radar. *Geophys. Res. Lett.*, 40, 11, 2567–2572. DOI: 10.1002/grl.50314
- Verdon, J.P., Kendall, J.M., Horleston, A.C. and Stork, A.L.: 2011, Subsurface fluid injection and induced seismicity in southeast Saskatchewan. *Int. J. Greenh. Gas Control*, 54, 2, 429–440. DOI: 10.1016/j.ijggc.2016.04.007
- Wang, W., Meng, X., Peng, Z., Chen, Q. and Liu, N.: 2015, Increasing background seismicity and dynamic triggering behaviors with nearby mining activities around Fangshan Pluton in Beijing, China. *J. Geophys. Res., Solid Earth*, 120, 8, 5624–5638. DOI: 10.1002/2015JB012235
- Wessel, P. and Smith, W.H.F.: 2013, Generic Mapping Tools: Improved version released. *EOS Trans. AGU*, 94, 45, 409–410. DOI: 10.1002/2013EO450001
- Yeck, W.L., Hayes, G.P., McNamara, D.E., Rubinstein, J.L., Barnhart, W.D., Earle, P.S. and Benz, H.M.: 2017, Oklahoma experiences largest earthquake during ongoing regional wastewater injection hazard mitigation efforts. *Geophys. Res. Lett.*, 44, 2, 711–717. DOI: 10.1002/2016GL071685
- Zembaty, Z.: 2004, Rockburst induced ground motion—a comparative study. *Soil Dyn. Earthq. Eng.*, 24, 1, 11–23. DOI: 10.1016/j.soildyn.2003.10.001